AIAA JOURNAL
Vol. 33, No. 1, January 1995

Turbulent Transonic Airfoil Flow Simulation Using a Pressure-Based Algorithm

Gang Zhou,* Lars Davidson,† and Erik Olsson‡
Chalmers University of Technology, S-412 96 Gothenburg, Sweden

There are few successful computational reports for transonic airfoil flow worked out with the pressure-based method. In this study, an advanced approach based on a pressure correction scheme is developed to solve the Reynolds-averaged Navier-Stokes equations for turbulent transonic flow around the airfoil RAE 2822. An implicit numerical dissipation model is adopted to create a dissipation mechanism based on pressure gradients to damp the destabilizing numerical effects, without smearing the physical discontinuity at shocks. The standard k-ϵ turbulence closure with a near-wall one-equation model is used. The computational results are compared with experimental data. Several discretization schemes such as the second-order upwind, hybrid, and MUSCL schemes for convection terms are investigated. The computational results show that the proposed pressure-based method has a resolution comparable to, or better than, the traditional time-marching methods.

I. Introduction

FOR a long time, most compressible aerodynamic flow simulations have been carried out with density-based methods (as time-marching methods are often called) in which density is used as a primary variable in the continuity equation, while pressure is extracted from the equation of the state. It is well known that this class of methods is inefficient for incompressible flow calculations because the density variation in these regions becomes negligible, leading to convergence problems. On the other hand, pressure-correction-based methods[1-4] that use pressure as a dependent variable show excellent performance in predicting incompressible turbulent and chemically reacting flow.

For transonic flow simulations, however, some difficulties have been encountered due to the complicated nature of the flow, including both subsonic and supersonic regions as well as shocks. In recent years, many improvements have been made for pressure-based methods, such as nonstaggered (collocated) grid arrangement,[5-12] the use of mass flux components (ρU, ρV) as primary variables[10-12] instead of velocities (U, V), and advanced numerical artificial dissipation models.[5,7,10-12] Some successful results have been reported. However, most of them deal with internal flow simulation. A few[12,13] successful calculations of transonic airfoil flow, which is the most challenging case for the demonstration of how well a pressure-based method can resolve physical discontinuities, such as external shocks, are available in the literature. In this work, a pressure-correction-based algorithm is demonstrated and validated for turbulent transonic airfoil flow computations using Reynolds-averaged Navier-Stokes equations.

Among all of the difficulties encountered when using the pressure-based method for predicting transonic flows, the most important issue is which type of and how much artificial dissipation should be included in the calculations to prevent the unphysical behavior that is caused by the elliptic nature of the pressure-correction equation. How well a computational algorithm can capture the physical discontinuities depends on a proper choice of a numerical dissipation model. For the transonic flow simulations, one must find a mechanism for introducing just enough artificial dissipation to damp the unphysical behavior without smearing the physical discontinuity at shocks. Many efforts have been focused on this.[3,5,7,9-12] For the density-based methods, it is well known that a proper numerical dissipation model[14-16] should be a combination of fourth- and second-order differencing of the dependent variables. Some successful pressure-based methods[7,10-12] have also demonstrated (some directly and others indirectly) a similar requirement for the dissipation model. This work uses an implicit artificial dissipation model that consists of second- and fourth-order differences of pressure only in all equations. The fourth-order terms of the numerical dissipation model are due to the use of Rhie-Chow interpolation,[2] and the second-order terms are due to the use of retarded density,[11,17] which is equivalent to the retarded pressure concept.[10]

Many turbulence models have been designed, such as algebraic turbulence models,[18,19] a number of k-ϵ models,[20] and Reynolds stress turbulence models (often referred to as second moment closure). The major objective here is not to implement a sophisticated turbulence model but rather to use a standard k-ϵ turbulence closure with a one-equation model near the wall. The results of the prediction of the transonic flow around airfoil RAE 2822 for case 6, case 9, and case 10 of Cook et al.[21] will be presented and discussed.

The main features of the proposed algorithm are the following:

1) Using a collocated grid arrangement in which all variables are stored at the center of the cell. Since the convection and diffusion contributions to the coefficients in the discretized equations are the same for all variables in this arrangement, it is attractive when employing high-order differencing schemes.

2) Solving for Cartesian mass flux components (ρU, ρV). Since mass flux components (ρU, ρV) vary more smoothly than the velocity components (U, V) across shocks, solving for mass flux components reduces discretization errors in the shock regions.

3) Assuming constant stagnation enthalpy everywhere in the flowfield. Since the maximum Mach number of the test cases is moderate (<1.4), it is reasonable to assume that the viscous dissipation is relatively low.

4) Adopting an implicit dissipation model, which mainly includes second- and fourth-order differencing terms expressed in pressure only.

5) Using varying local time step to enhance the numerical stability and convergencing.

6) Standard two-equation turbulence closure with a near-wall one-equation model.

7) Several schemes, such as hybrid, second-order upwind, and MUSCL, for convective terms.

II. Governing Equations and Turbulent Closure

The transonic mean flow is modeled by the Reynolds-averaged conservation equations of mass, momentum, and energy. These

Received April 5, 1994; revision received Aug. 16, 1994; accepted for publication Aug. 19, 1994.

*Research Student, Department of Thermo and Fluid Dynamics. Member AIAA.
†Associate Professor, Department of Thermo and Fluid Dynamics.
‡Professor, Department of Thermo and Fluid Dynamics.

mean equations, in terms of the Favre-averaged concept, can be expressed in Cartesian tensor form for ideal gas as[22]

$$\bar{\rho}_{,t} + (\bar{\rho}\tilde{u}_j)_{,j} = 0 \tag{1}$$

$$(\bar{\rho}\tilde{u}_i)_{,t} + [\bar{\rho}\tilde{u}_j\tilde{u}_i + \delta_{ij}\bar{P} - (\bar{\tau}_{ij} - \overline{\rho u_i'' u_j''})]_{,j} = 0 \tag{2}$$

$$(\bar{\rho}\tilde{H} - \bar{P})_{,t} + [\tilde{u}_j(\bar{\rho}\tilde{H}) + \bar{q}_j + \overline{\rho u_j'' h''}]_{,j} - [\tilde{u}_i(\bar{\tau}_{ij} - \overline{\rho u_i'' u_j''})]_{,j} = 0 \tag{3}$$

where

$$\bar{\tau}_{ij} = \mu\left(\tilde{u}_{i,j} + \tilde{u}_{j,i} - \tfrac{2}{3}\delta_{ij}\tilde{u}_{m,m}\right) \tag{4}$$

$$\bar{\rho} = \frac{\gamma\bar{P}}{(\gamma-1)(\tilde{H} - 0.5\tilde{u}_i\tilde{u}_i)} \tag{5}$$

where $\bar{\rho}$ is the mean density, $\bar{P}$ the mean pressure, $\tilde{u}_i$ the mean velocity in the direction of x_i, $\tilde{H}$ the total enthalpy per unit mass, and μ the coefficient of molecular viscosity. In the previous equations, the overbar $(-)$ denotes Reynolds averaging, and tilde $(\sim)$ denotes Favre averaging.

It will be assumed that the ratio of specific heats γ is constant and that total enthalpy may be considered to be constant. Such an assumption is reasonable for the present moderate Mach number ($M \prec 1.4$)[23] cases. This assumption avoids solving the energy equation and modeling of turbulent heat fluxes. Therefore, the closure of the Reynolds-averaged equations only requires the modeling of Reynolds stresses. Here the Boussinesq eddy viscosity assumption is used to express the Reynolds stresses tensor as

$$\overline{\rho u_i'' u_j''} = -\mu_t\left[\tilde{u}_{i,j} + \tilde{u}_{j,i} - \tfrac{2}{3}\delta_{ij}\tilde{u}_{m,m}\right] + \tfrac{2}{3}\delta_{ij}\bar{\rho}\tilde{k} \tag{6}$$

where μ_t is the eddy viscosity, and $\tilde{k}$ is the turbulent kinetic energy per unit mass:

$$\bar{\rho}\tilde{k} = \tfrac{1}{2}\overline{\rho u_i'' u_i''} \tag{7}$$

The values of the eddy viscosity μ_t are estimated by solving two transport equations for the turbulent kinetic energy $\tilde{k}$ and its dissipation rate ϵ:

$$(\bar{\rho}\tilde{k})_{,t} + \left[\tilde{u}_j(\bar{\rho}\tilde{k}) - \left(\mu + \frac{\mu_t}{\sigma_k}\right)\tilde{k}_{,j}\right]_{,j} = P_k - (\bar{\rho}\tilde{\epsilon}) \tag{8}$$

$$(\bar{\rho}\tilde{\epsilon})_{,t} + \left[\tilde{u}_j(\bar{\rho}\tilde{\epsilon}) - \left(\mu + \frac{\mu_t}{\sigma_\epsilon}\right)\tilde{\epsilon}_{,j}\right]_{,j} = \frac{\tilde{\epsilon}}{\tilde{k}}[c_{1\epsilon}P_k - c_{2\epsilon}(\bar{\rho}\tilde{\epsilon})] \tag{9}$$

where the production term has the form

$$P_k = -\overline{\rho u_i'' u_j''}\tilde{u}_{i,j} \tag{10}$$

and the eddy viscosity, away from the wall, is modeled as

$$\mu_t = c_\mu\bar{\rho}\frac{\tilde{k}^2}{\epsilon} \tag{11}$$

A near-wall one-equation model[24,25] for the turbulent kinetic energy is applied in this study, which in the literature has been used both together with the k-ϵ model[7,22] and second moment closure.[26–28] The model defines two different length scales l_μ and l_ϵ, one for turbulent stress and one for turbulent dissipation. Then the dissipation rates of the turbulent kinetic energy and the eddy viscosity are modeled by

$$\tilde{\epsilon} = \frac{\tilde{k}^{\frac{3}{2}}}{l_\epsilon}; \qquad \mu_t = \bar{\rho}c_\mu\tilde{k}^{\frac{1}{2}}l_\mu \tag{12}$$

Therefore, close to the wall, the closure of the Reynolds-averaged equations with the one-equation model is reduced to solving the k equation and specifying the turbulent dissipation length scale l_ϵ and turbulent length scale l_μ. An exponential expression[24,25] is used to combine the viscous sublayer and inner-layer dissipation length scale and turbulent length scales as

$$l_\epsilon = C_l y_n\left[1 - \exp\left(\frac{-\tilde{k}^{\frac{1}{2}}y_n}{2C_l\nu}\right)\right] \tag{13}$$

$$\ell_\mu = C_l y_n\left[1 - \exp\left(\frac{-\tilde{k}^{\frac{1}{2}}y_n}{A_\mu\nu}\right)\right] \tag{14}$$

$$C_l = \kappa C_\mu^{-\frac{3}{4}}, \qquad A_\mu = 70 \tag{15}$$

where y_n is the normal distance from the wall. The matching position between the viscous sublayer and the outer region is chosen along a fixed grid line where the value of the term $\tilde{k}^{\frac{1}{2}}y_n/\nu$ is of order 250.

In the present turbulent closure modeling, the constants are

$$c_\mu = 0.09; \quad c_{1\epsilon} = 1.44; \quad c_{2\epsilon} = 1.92; \quad \sigma_k = 1.0; \quad \sigma_\epsilon = 1.3 \tag{16}$$

III. Numerical Approach

The governing equations given earlier can be cast into the standard transport equation for a general dependent variable Φ (in the following section the bars indicating the averaging are dropped) in Cartesian coordinates as

$$\Phi_{,t} + (U_i\Phi)_{,i} = \left[\Gamma_\Phi\left(\frac{\Phi}{\rho}\right)_{,i}\right]_{,i} + S^\Phi \tag{17}$$

where Φ can be the Cartesian mass flux components, turbulent kinetic energy, dissipation rate of turbulent kinetic energy, etc.; Γ_Φ is the effective diffusivity; and S_Φ denotes the source per unit volume for the dependent variables Φ.

A. Discretization

Integrating Eq. (17) over a control volume, by using the Gaussian theorem, we get the following discretized equation,

$$(\Phi - \Phi^0)\frac{\delta v}{\Delta t} + \sum_m(\boldsymbol{F}\cdot\boldsymbol{A}) - \sum_m\left[\Gamma_\Phi\nabla\left(\frac{\Phi}{\rho}\right)\cdot\boldsymbol{A}\right] = S_\Phi\delta v \tag{18}$$

where $\boldsymbol{F} = (\rho\boldsymbol{V}, \boldsymbol{V}\Phi)^T$ is the flux tensor, δv is the volume of the cell, Φ^0 is the value at previous time level, and m refers to each face $\boldsymbol{A}$ of the control volume. The discretizing equation can be cast into standard form (see Refs. 8 and 12)

$$a_P\Phi_P = \sum a_{nb}\Phi_{nb} + S_C^\Phi \tag{19}$$

where subscript nb denotes neighbor and

$$a_P = \sum a_{nb} - S_P^\Phi \tag{20}$$

The coefficients a_{nb} contain contributions from both convection and diffusion; S_C^Φ and S_P^Φ contain the remaining terms. When Eq. (18) is cast into the form of Eq. (19), some additional source terms S_C^Φ and S_P^Φ must be considered,[29] due to the choice of dependent variables as mass flux components.

The first additional term is referred to as the convecting source term that represents the volume flux from the convection parts of coefficients a_{nb} over the control volume[1] when computing a_P in Eq. (20). It can be written

$$\left(S_P^\Phi\right)_{\text{add1}} = \sum_m\left[\frac{(\rho\boldsymbol{V})\cdot\boldsymbol{A}}{\tilde{\rho}}\right]_m$$

Note that this term is the continuity error when solving for the velocity components. It should be pointed out also that to balance the discretized equation the retarded density[17] $\tilde{\rho}$ should be used in

the term $(S_P^\Phi)_{\text{add1}}$, since the right-hand side of Eq. (19) has adopted the numerical model that includes the retarded density.

The second additional term is referred to as the diffusion source term, due to the adoption of a description of the stress tensor in Eqs. (4) and (6). This term

$$\left(S_C^\Phi\right)_{\text{add2}} = \left[(\mu + \mu_t)\left(\tilde{u}_{j,i} - \tfrac{2}{3}\delta_{ij}\tilde{u}_{m,m}\right)\right]_{,j} - \tfrac{2}{3}\delta_{ij}\left(\tilde{\rho}\tilde{k}\right)_{,j}$$

is added to S_C^Φ.

The third additional term is referred to as the compressible source term due to a decoupling of the derivative of mass flux and velocity. It is shown explicitly as follows:

$$\Gamma_\Phi \frac{\partial}{\partial x_j}\left(\frac{\Phi}{\rho}\right) = \frac{\Gamma_\Phi}{\rho}\frac{\partial \Phi}{\partial x_j} + \frac{\Gamma_\Phi \Phi}{\rho^2}\frac{\partial \rho}{\partial x_j}$$

The third source term consists of the second term on the right-hand side in the previous equation.

It should be noticed that the first term $((S_P^\Phi)_{\text{add1}})$ is crucial to momentum conservation and numerical stability. At shocks, the third source term is also important.

B. Numerical Dissipation

There are a variety of numerical dissipation models that are used to suppress spurious odd and even point oscillations and to damp unphysical overshoots near shock waves. Most of them use a combination of second- and fourth-order terms of the dependent variables Φ, (ρ, ρU, ρV, and ρE), either explicitly or implicitly. In this study, an implicit numerical dissipation model is used that just includes the second- and fourth-order terms expressed in pressure for all transport equations. For uniform grid and two-dimensional flow, the model can be written explicitly[12,29]

$$DP = D_x P + D_y P \tag{21}$$

where $D_x P$ and $D_y P$ are the contributions for the two coordinate directions, respectively, which have the following form (for U_η, $U_\xi > 0$):

$$\begin{aligned} D_x P &= \left(d_{i+\frac{1}{2},j} - d_{i-\frac{1}{2},j}\right) \\ D_y P &= \left(d_{i,j+\frac{1}{2}} - d_{i,j-\frac{1}{2}}\right) \end{aligned} \tag{22}$$

The various d in the previous equations can be written

$$\begin{aligned} d_{i+\frac{1}{2},j} &= A_x \mu_{i+\frac{1}{2}}\left(P_{i+\frac{1}{2},j} - P_{i-\frac{1}{2},j}\right) \\ &\quad + B_x(P_{i+2,j} - 3P_{i+1,j} + 3P_{i,j} - P_{i-1,j}) \end{aligned} \tag{23}$$

where A and B are coefficients imposed by momentum and state equations, and $\mu_{i+\frac{1}{2}}$ is a smoothing function due to the use of retarded density[17] that reads

$$\tilde{\rho} = \rho - \mu \Delta x \bar{\rho}_x \tag{24}$$

A two-level filtering smoothing function has been designed[12,29] as

$$\begin{aligned} \mu_{i+\frac{1}{2}} = \max\Bigg\{ & 0.0, K_1\left[1 - \left(\frac{M_{\text{ref}}}{M_{i+\frac{1}{2},j}}\right)^2\right] \\ & + K_2\left[1 - \left(\frac{\Upsilon_{\text{ref}}}{\Upsilon_{i+\frac{1}{2},j}}\right)^2\right]\Bigg\} \end{aligned} \tag{25}$$

where

$$\Upsilon_{i+\frac{1}{2},j} = \max(\Upsilon_{i+1,j}, \Upsilon_{i,j})$$

and

$$\Upsilon_{i,j} = \frac{|P_{i+1,j} - 2P_{i,j} + P_{i-1,j}|}{|P_{i+1,j} + 2P_{i,j} + P_{i-1,j}|}$$

It was found that only one level filter is needed for turbulent flow calculations to switch on the second-order dissipation that is needed to enhance the stability in supersonic regions.

The constants are set as $K_1 = 1$, $K_2 = 0$, and $M_{\text{ref}} = 1.0$–1.06. The details of the present model are given in the Appendices in Refs. 12 and 29.

C. Pressure-Correction Equation

In this study, mass flux components instead of velocities are selected as the dependent variables. Such a variable option allows for a direct relationship between momentum and pressure by truncating the momentum equations in the same way as in the conventional SIMPLE method[1,8]

$$\mathbf{A} \cdot (\rho V)' = -\frac{\delta v}{a_P} \mathbf{A} \cdot \nabla P' \tag{26}$$

where $'$ means correction terms.

To enhance stability of the original pressure-correction equation, the density correction is taken as[10]

$$\rho' = \frac{\gamma P'}{(\gamma - 1)\left(H_0 - 0.5|V|^2\right)} \tag{27}$$

Therefore, the pressure-correction equation becomes

$$\rho_P' \frac{\delta v}{\Delta t} + \sum_{m=1}^{4}\left(\frac{\delta v}{a_P}\mathbf{A} \cdot \nabla P'\right) + \Delta \dot{m}_P = 0 \tag{28}$$

where $\Delta \dot{m}_P$ is the continuity error.

This manipulation gives the pressure-correction equation a hyperbolic appearance with respect to time. As the Mach number becomes small and density gradients become negligible, the quasi-time-dependent term disappears, and the scheme degenerates to the standard iterative scheme for incompressible flow.

The discretized equation for P' can also be cast into the form

$$a_P P_P' = \sum a_{nb} P_{nb}' + S_C \tag{29}$$

where S_C is mass residual.

D. Initial and Boundary Conditions

The calculations are started from a uniform freestream condition for all variables.

At the far field, the locally one-dimensional Riemann invariants, entropy, and tangential velocity component are obtained by using the theory of characteristics. A far-field circulation correction based on the compressible potential vortex solution is used to modify freestream velocity. The Neumann boundary condition is used at all boundaries for the pressure correction, and first-order extrapolation (the second normal derivative equal to zero) is used for the pressure. On solid walls, no-slip and zero turbulent energy boundary conditions are applied. The values of k and ϵ at the outlets are extrapolated from the inner field.

IV. Results and Discussion

Three calculation cases are examined for airfoil RAE 2822, which has been extensively investigated experimentally by Cook et al.[21] and computationally by many aerodynamists. All cases use a 256 × 64 C grid with 208 cells on the airfoil's surface and finer clustering near the leading and trailing edges. The grid extent is about 10 chords in all directions. The normal spacing of the first point off the wall is on the order 1×10^{-5} of the chord that corresponds to $0(y^+)$. For all cases the pure MUSCL[31,33] scheme (the term "pure" means that the MUSCL scheme is used for all equations, i.e., the convective terms of both momentum and k-ϵ equations) is adopted first. Then the calculations using the pure hybrid scheme[1] and second-order upwind schemes LUDS[32,33] are adopted.

In the first case referred to as case 6 of Ref. 21 $M = 0.725$, $R_e = 6.5 \times 10^6$, and the flow is at an angle of attack $\alpha = 2.92$ deg (uncorrected). The transition location for this case is fixed at $x/C = 0.03$, the same as in the experimental data. Since the calculations are carried out in free flow, the angle of attack must be corrected

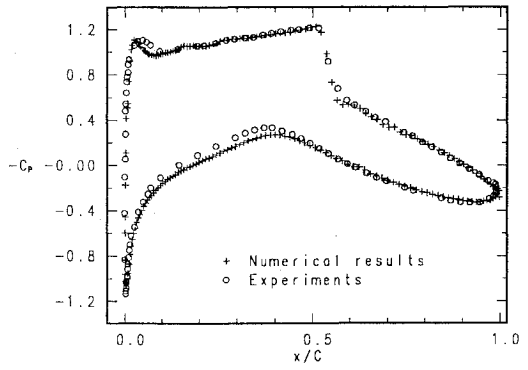

Fig. 1 Pressure distributions for RAE 2822, case 6, MUSCL scheme.

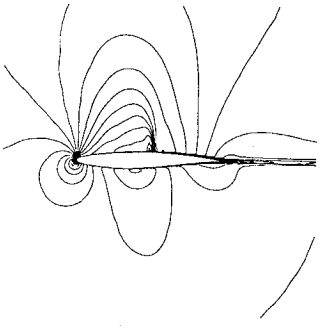

Fig. 2 Mach number contours, case 6, MUSCL scheme.

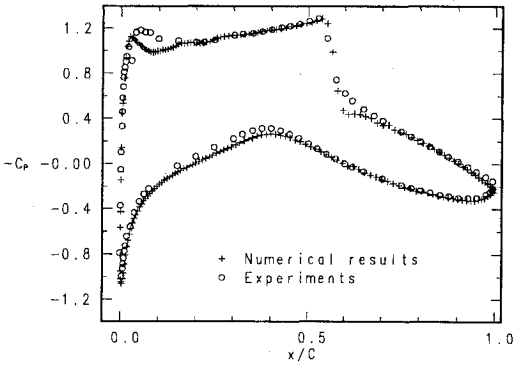

Fig. 3 Pressure distributions for RAE 2822, case 9, MUSCL scheme.

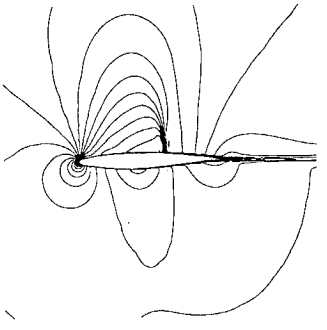

Fig. 4 Mach number contours, case 9, MUSCL scheme.

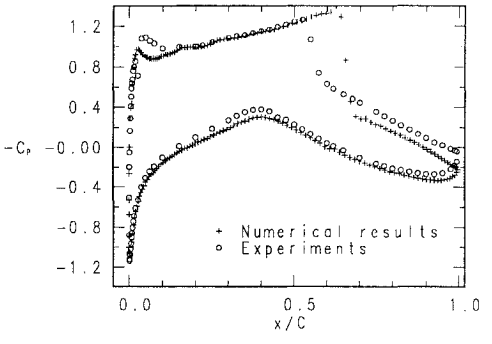

Fig. 5 Pressure distributions for RAE 2822, case 10, MUSCL scheme.

from the geometrical angle of attack due to the presence of wind-tunnel interference. Various types of correction on Mach number and angle of attack have been proposed in airfoil flow simulation.[30] In this calculation, the corrected angle of attack is chosen as $\alpha = 2.60$, which is the same as in Ref. 13, whereas no correction is made for the freestream Mach number. Figure 1 shows the pressure coefficient distributions on the upper and lower airfoil surfaces from the present calculations in comparison with experiment data. The Mach number contours are shown in Fig. 2.

It can be seen that the computed results show good agreement with the experiments. A sharp discontinuity is achieved successfully for both shock strength and location. On the lower surface of the airfoil the pressure is slightly overpredicted. Such a feature is common in almost all of the computational results in Ref. 30. The results shown in Ref. 13, which also used the pressure-based method, are in better agreement with experiments on the lower surface of this airfoil, but the shock strength and location were less well predicted.

Another difficulty in this computation, apart from the shock region, is a proper prediction of pressure distribution in the transition region on the upper surface of the airfoil. The presented results show that the peak at the transition point and the wavy pattern of pressure on the upper surface agree very well with experiments. Just after the transition point, pressure is slightly overpredicted.

The second case presented corresponds to case 9 of Ref. 21, in which $M = 0.73$, $R_e = 6.5 \times 10^6$, and $\alpha = 3.19$ deg (uncorrected). The transition location is at $x/C = 0.03$. The corrected angle of attack is chosen as $\alpha = 2.80$. The computed pressure coefficient is compared with the experiment in Fig. 3. Mach number contours are shown in Fig. 4. Again, a good agreement with experiments is achieved for both shock strength and location. Downstream of the transition point, the wavy pattern of pressure shows a tendency similar to that in experimental data. It can be seen that the discrepancy between numerical results and experiments just after the transition point increases.

The last case referred to as case 10 of Ref. 21 is $M = 0.75$, $R_e = 6.2 \times 10^6$, and $\alpha = 3.19$. This is the most difficult RAE 2822 case, since the shock wave causes a significant amount of boundary-layer separation. In this calculation, the corrected angle of attack is chosen as $\alpha = 2.57$. Figure 5 compares computed pressure coefficient distribution with experimental data. Almost all of the calculations have overpredicted the shock strength and the location.[22,28,30] The presented results also show the same tendency. After the shock on the upper surface of the airfoil the pressure is overpredicted similarly to the results obtained from any of the density-based methods. This indicates that the numerical error involved in the pressure-based method is of comparable order to that in the time-marching method for this case.

On the other hand, the fact that both pressure-based and density-based methods overpredict the shock strength and its location indicates that the discrepancy between numerical results and experiments in the case with the strong shock must be due to modeling errors, i.e., the turbulence model, or experimental uncertainties. The Mach numbers are shown in Fig. 6.

To investigate the difference in performance between different schemes, hybrid[1] and second-order linear upwind schemes (LUDS)[32,33] are also used for calculating all of the cases. Results show that there are no significant differences between these schemes in the global results and the pattern of isolines of Mach number and pressure. Figures 7–9 show the predicted pressure coefficient distribution using the second-order upwind scheme.

The unbounded second-order upwind scheme shows an impressive ability to predict pressure distribution on almost the entire surface of the airfoil in all cases, except for a slightly retarded prediction of the shock location. No numerical stability problems occur. The most interesting performance of the second-order upwind scheme is that the scheme can capture the negative pressure peak at the transition point in a much better way than MUSCL and hybrid schemes. This typical higher order upwinding performance is also shown in

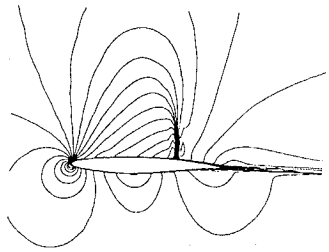

Fig. 6 Mach number contours, case 10, MUSCL scheme.

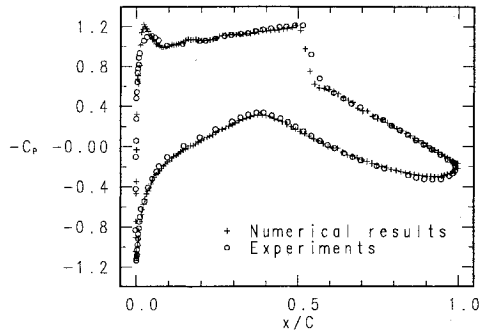

Fig. 7 Pressure distributions for RAE 2822, case 6, LUDS scheme.

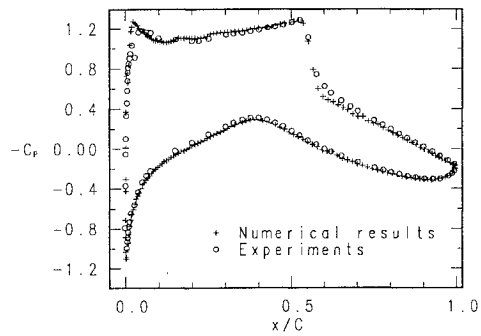

Fig. 8 Pressure distributions for RAE 2822, case 9, LUDS scheme.

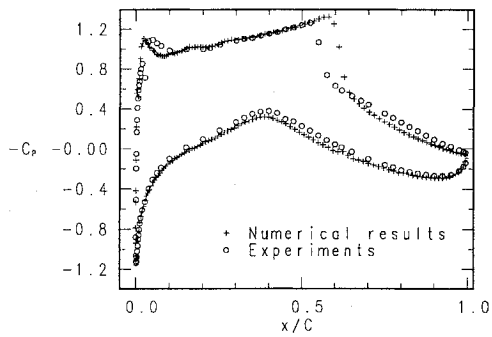

Fig. 9 Pressure distributions for RAE 2822, case 10, LUDS scheme.

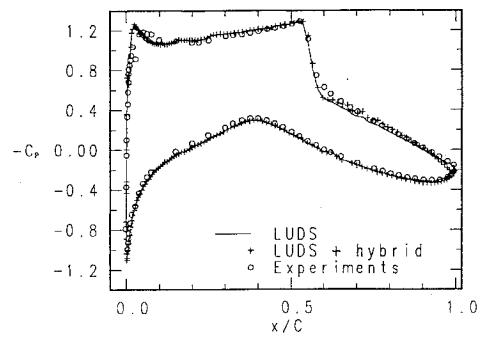

Fig. 10 Pressure distributions for RAE 2822, case 9, comparison between LUDS and LUDS/hybrid schemes.

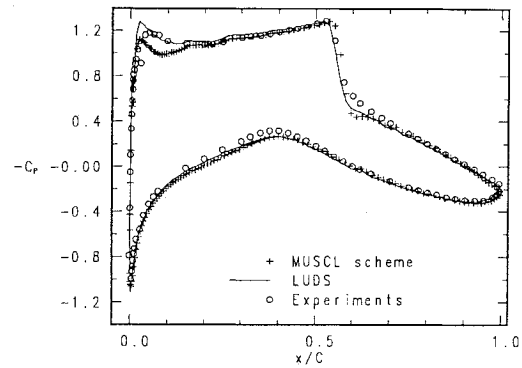

Fig. 11 Pressure distributions for RAE 2822, case 9, comparison between MUSCL and LUDS schemes with same constant, $M_{ref} = 1.04$.

Ref. 34 in which third-order upwinding schemes are used. Note that the predicted negative pressure peak pierces through experiment data. Considering that the predicted pressure distribution just after the transition point follows data with a satisfactory accuracy, this sharper peak might be acceptable since there is a sharp stimulus at the transition point.

Figure 10 shows the comparison between the results obtained from a pure second-order upwind scheme and those from the combination of a hybrid scheme for the k-ϵ equations and a second-order upwind scheme for momentum equations. From this figure we can see that there is no significant difference between these two computations. The reason for this is the fact that k-ϵ equations are dominated by diffusion and source terms. Therefore, the choice of a discretization scheme for relatively small convection terms does not influence the global calculated flowfield much. Nevertheless, the resolution of the pressure just after the transition point is lower in the latter computation.

It is noticed that the computational results are not very sensitive to the numerical constant M_{ref} even though it was shown that the perfect conditions are $K = 1.0$, and $M_{ref} = 1.04$ for MUSCL and $K = 1.0$ and $M_{ref} = 1.05$ for LUDS. Figure 11 shows a comparison of MUSCL and LUDS schemes with the same constant ($M_{ref} = 1.04$). The main difference is in the resolution of the pressure at the transition region. MUSCL is a combination of the central differencing and the second-order linear upwinding. It is believed that MUSCL switches on central differencing in the reverse pressure gradient region, leading to averaging of the flowfield and smearing the negative peak, in the transition region. Comparing Figs. 10 and 11, one can see that a change in M_{ref} from 1.04 to 1.05 does not have any significant influence on the LUDS predictions.

V. Concluding Remarks

A pressure-based method using a k-ϵ turbulence closure with a one-equation model near the wall has been presented to calculate the turbulent transonic flow over an airfoil. An implicit nonlinear dissipation model was successfully used in different discretization schemes to suppress oscillation without smearing the physical discontinuity at shocks. To substantiate the validity of the proposed method, three calculations for the airfoil RAE 2822 have been carried out. The computational results obtained from the proposed method, with several discretization schemes, have shown a good agreement with experimental data compared with density-based methods. Among the schemes adapted, the second-order upwind scheme has shown the sharpest behavior.

One important conclusion that can be drawn from this work is that an advanced pressure-based method is also capable of predicting turbulent transonic aerodynamic flows around airfoils, even though its popularity is due mainly to its excellent performance in predicting incompressible turbulent flows. The convergence rate is rather slow. To obtain a fully converged solution requires approximately 13,000 time steps, which takes 26 hours on a small Alpha-machine (DEC 3000/400). Some improvement including convergence acceleration and advanced turbulence modeling should be undertaken for the proposed method in the future.

References

[1]Patankar, S. V., *Numerical Heat Transfer and Fluid Flow*, McGraw-Hill, Washington, DC, 1980.

[2]Rhie, C. M., "A Pressure Based Navier-Stokes Solver Using the Multigrid Method," AIAA Paper 86-0207, Jan. 1986.

[3]Karki, K. C., and Patankar, S. V., "Pressure Based Calculation Procedure for Viscous Flows at All Speeds in Arbitrary Configurations," *AIAA Journal*, Vol. 27, 1989, pp. 1167–1174.

[4]Shyy, W., and Chen, M. H., "Pressure-Based Multigrid Algorithm for Flow at All Speeds," *AIAA Journal*, Vol. 30, 1992, pp. 2660–2669.

[5]Rhie, C. M., and Chow, W. L., "Numerical Study of the Turbulent Flow Past an Airfoil with Trailing Edge Separation," *AIAA Journal*, Vol. 21, 1984, pp. 1527–1532.

[6]Perić, M., "A Finite Volume Method for the Prediction of Three-Dimensional Fluid Flow in Complex Ducts," Ph.D. Thesis, Univ. of London, London, 1985.

[7]Chen, Y. S., "Viscous Flow Computations Using a Second-Order Upwind Differencing Scheme," AIAA Paper 88-0417, Jan. 1988.

[8]Davidson, L., and Farhanieh, B., "A Finite-Volume Code Employing Collocated Variable Arrangement and Cartesian Velocity Components for Computation of Fluid Flow and Heat Transfer in Complex Three-Dimensional Geometries," Thermo and Fluid Dynamics, Chalmers Univ. of Technology, Rept. 92/4, Gothenburg, Sweden, 1992.

[9]Zhou, G., and Davidson, L., "Transonic Flow Computation Using a Modified SIMPLE Code Based on Collocated Grid Arrangement," *Proceedings of the First European Computational Fluid Dynamics Conference* (Brussels), Vol. 2, 1992, pp. 749–756.

[10]Mcguirk, J. J., and Page, G. J., "Shock Capturing Using a Pressure-Correction Method," *AIAA Journal*, Vol. 28, 1990, pp. 1751–1757.

[11]Lien, F. S., and Leschziner, M. A., "A Pressure-Velocity Solution Strategy for Compressible Flow and Application to Shock/Moment Turbulence Closure," *Journal of Fluid Engineering*, Vol. 115, 1993, pp. 717–725.

[12]Zhou, G., and Davidson, L., "A Pressure Correction Based Euler Scheme for Internal and External Transonic Flow Simulation," *Journal of Computational Fluid Dynamics* (to be published, 1995).

[13]Lai, Y. G., So, R. M. C., and Przekwas, A. J., "Aerodynamic Flow Simulation Using a Pressure-Based Method and a Two-Equation Turbulence Model," AIAA Paper 93-2902, July 1993.

[14]Jameson, A., Schmidt, W., and Turkel, E., "Numerical Solutions of the Euler Equations by Finite Volume Methods Using Runge-Kutta Time-Stepping Schemes," AIAA Paper 81-1259, June 1981.

[15]Rizzi, A., "Spurious Entropy and Very Accurate Solutions to the Euler Equations," AIAA Paper 84-1644, Jan. 1984.

[16]Pulliam, T. H., and Barton, J. T., "Euler Computations of AGARD Working Group 07 Airfoil Test Cases," AIAA Paper 85-0018, Jan. 1985.

[17]Wornom, S. F., and Hafez, M., "Calculation of Quasi-One-Dimensional Flows with Shocks," *Computers and Fluids*, Vol. 14, No. 2, 1986, pp. 131–140.

[18]Cebeci, T., and Smith, A. M. O., *Analysis for Turbulent Boundary Layers*, Academic Press, New York, 1974.

[19]Baldwin, B., and Lomax, H., "Thin-Layer Approximation and Algebraic Model for Separated Turbulent Flows," AIAA Paper 78-257, Jan. 1978.

[20]Patel, V. C., Rodi, W., and Scheuerer, G., "Turbulent Models for Near-Wall and Low Reynolds Number Flows: A Review," *AIAA Journal*, Vol. 23, 1985, pp. 1308–1318.

[21]Cook, P. H., McDonald, M. A., and Firmin, M. C. P., "Aerofoil RAE 2822—Pressure Distributions, and Boundary Layer and Wake Measurements," AGARD Advisory Rept. 138, 1979.

[22]Mitcheltree, R. A., Salas, M. D., and Hassan, H. A., "One-Equation Turbulence Model for Transonic Airfoil Flows," *AIAA Journal*, Vol. 28, 1990, pp. 1625–1632.

[23]Lien, F. S., "Computational Modeling of 3D Flow in Complex Ducts and Passages," Ph.D. Thesis, Feb. 1992.

[24]Wolfshtein, M., "The Velocity and Temperature Distribution in One-Dimensional Flow with Turbulence Augmentation and Pressure Gradient," *International Journal of Mass Heat Transfer*, Vol. 12, 1969, pp. 301–318.

[25]Chen, H. C., and Patel, V. C., "Practical Near-Wall Turbulence Models for Complex Flow Including Separation," AIAA Paper 87-1300, June 1987.

[26]Davidson, L., and Rizzi, A., "Navier-Stokes Computation of Airfoil in Stall Using Algebraic Reynolds-Stress Model," *Journal of Spacecraft and Rockets*, Vol. 79, 1992, pp. 794–800.

[27]Davidson, L., "Reynolds Stress Transport Modeling of Shock/ Boundary-Layer Interaction," AIAA Paper 93-2936, July 1993.

[28]Hellström, T., Davidson, L., and Rizzi, A., "Reynolds Stress Transport Modeling of Transonic Flow Around the RAE 2822 Airfoil," AIAA Paper 94-0309, Jan. 1994.

[29]Zhou, G., "Numerical Simulation for Transonic Flows with Special Emphasis on Development of Pressure-Based Method to Aerodynamic Flow," Thermo and Fluid Dynamics, Chalmers Univ. of Technology, Lic. Thesis for Engi., Rept. 93/94, Gothenburg, Sweden, 1993.

[30]Holst, T. L., "Viscous Transonic Airfoil Workshop Compendium of Results," *AIAA Journal*, Vol. 25, 1988, pp. 1073–1087.

[31]van Leer, B., "Towards the Ultimate Conservation Difference Scheme V, A Second-Order Sequel to Godunov's Method," *Journal of Computational Physics*, Vol. 32, 1979, p. 101.

[32]Shyy, W., Thakur, S., and Wright, J., "Second-Order Upwind and Central Difference Schemes for Recirculating Flow Computation," *AIAA Journal*, Vol. 30, 1992, pp. 923–932.

[33]Lien, F.-S., and Leschziner, M. A., "Approximation of Turbulence Convection in Complex Flows with a TVD-MUSCL Scheme," *Proceedings of the Fifth International IAHR Symposium on Refined Flow Modeling and Turbulence Measurements* (Paris), 1993, pp. 183–190.

[34]Zhou, G., Davidson, L., and Olsson, E., "Transonic Inviscid/Turbulent Airfoil Flow Simulations Using a Pressure Based Method with High Order Schemes," 14th International Conference on Numerical Method in Flow Dynamics, Bangalore, India, July 1994.